Kinetics of $P2X_7$ Receptor-Operated Single Channels Currents

T. Riedel,* I. Lozinsky,† G. Schmalzing,‡ and F. Markwardt*
*Julius-Bernstein-Institute for Physiology, Martin-Luther-University Halle, Halle/Saale, Germany; †Department of Internal Medicine, University of Kentucky, Lexington, Kentucky; and ‡RWTH Aachen University, Department of Molecular Pharmacology, Aachen, Germany

ABSTRACT Human $P2X_7$ receptors were expressed in *Xenopus laevis* oocytes and single channels were recorded using the patch-clamp technique in the outside-out configuration. ATP^{4-} evoked two types of $P2X_7$ receptor-mediated single channel currents characterized by short-lived and long-lived openings. The short- and long-lasting open states had mean open times of ~5 and ~20 ms and slope conductances near −60 mV of 9 and 13 pS, respectively. The open probabilities of the short and long openings were strongly [ATP^{4-}]-dependent with EC_{50} values of ~0.3 mM and ~0.1 mM ATP^{4-}, respectively. The channel kinetics did not change significantly during sustained $P2X_7$ receptor activation for several minutes, as was also observed in recordings in the cell-attached patch-clamp configuration. Activation and deactivation of the short openings followed exponential time courses with time constants in the range of 20 ms, and displayed a shallow [ATP^{4-}] dependence of the activation process. The kinetics of the short channel openings at negative membrane potentials fitted well to a linear C-C-C-O model with two ATP^{4-} binding steps at equal binding sites with a dissociation constant K_d of 139 μM.

INTRODUCTION

Purinergic $P2X_7$ receptors belong to the P2X family of ligand-gated ion channels, which open in response to extracellular ATP, allowing small cations to pass passively in a nonselective manner through a transmembrane channel. $P2X_7$ receptors are highly expressed in cells of the immune and inflammatory system. ATP, released from different cells under hypoxic conditions or during cell destruction or necrosis, is believed to act as a danger signal to the immune system and to exert proinflammatory and immunomodulatory functions by binding to and activating $P2X_7$ receptors. For example, $P2X_7$ receptors have been shown to be involved in the killing of intracellular bacteria and release of interleukin-1β from macrophages (1).

$P2X_7$ receptors possess peculiar characteristics that distinguish them from the other members of the P2X receptor family, such as a C-terminal tail that is 200 amino-acids longer and the capacity to form a large cytolytic pore upon sustained activation (2). The time course of activation and deactivation of whole-cell currents evoked by activation of recombinant $P2X_7$ receptors or native $P2X_7$-like receptors varies greatly with species, agonist concentration, duration of agonist application, and concentration of divalent cations such as Ca^{2+} or Mg^{2+} (3). Thus, $P2X_7$ receptor-dependent or $P2X_7$-like current kinetics have been described as exponentially activating (4–7), biphasic fast and slowly activating (8–13), partially inactivating (13–17), or as being kinetically even more complex (18,19). Similarly, current deactivation was observed to follow a monoexponential time course with time constants <1 s (4–7,11), or to occur nonexponentially with a delay of up to several minutes (2,9,14,18,19). Repeated long-term agonist stimulations have been found to elicit either almost constant whole cell current amplitudes (4,11), or successively increasing currents (5,11,16,20,21), or decreasing current amplitudes (14,16). These contrary results have been interpreted to result from 1), activation-dependent long-lasting changes of the $P2X_7$ receptor conformation; 2), activation of ion channels activated downstream of the $P2X_7$ receptor (3); or 3), the existence of distinct activation sites for ATP on the $P2X_7$ receptor (12).

Millimolar concentrations of ATP are required for full activation of $P2X_7$ receptor-mediated inward currents. The observation that the ATP concentration for half-maximal activation (EC_{50}) of $P2X_7$ receptors is markedly lowered by reduction of the extracellular concentration of divalent cations is usually interpreted to indicate that free ATP^{4-} is the genuine receptor agonist (3,22). However, even when based on free ATP^{4-} concentrations, EC_{50} values as different as 3 μM (14) and 0.4 mM (11) have been reported. Again, these discrepancies may be attributed to cell type or condition-specific factors that affect peculiar $P2X_7$ receptor conformations by inducing lasting metabolic changes such as phosphorylation, resulting in altered agonist potency. Other possible explanations are that second messengers are produced in response to $P2X_7$ receptor activation that, by themselves, activate ion channels, or that ATP directly activates additional purinergic receptors distinct from $P2X_7$ receptors. As highly specific $P2X_7$ receptor antagonists are not yet available, electrophysiological recordings in the whole cell configuration do not really allow for discrimination between the different possibilities outlined above.

The goal of this study was to provide the first analysis of recombinant $P2X_7$ receptors at the single channel level and to develop a simple kinetic model of its function. In the excised outside-out patch configuration, $P2X_7$ receptor-mediated currents can be recorded under better-controlled conditions than achievable in the whole cell configuration

Submitted June 26, 2006, and accepted for publication December 11, 2006.
Address reprint requests to F. Markwardt, Tel.: 49-345-557-1390; E-mail: fritz.markwardt@medizin.uni-halle.de.
© 2007 by the Biophysical Society
0006-3495/07/04/2377/15 $2.00
doi: 10.1529/biophysj.106.091413

and can be clearly separated from any contaminating current component. Moreover, because of their small size and the surrounding very thin, unstirred layer of solution, outside-out patches are amenable to rapid solution exchange, enabling time-resolved recording of the rapid time course of activation and deactivation of $P2X_7$ receptors. The data provide a basis for further studies aimed at elucidating structure-function relationships of the $P2X_7$ receptor.

MATERIALS AND METHODS

Chemicals

Chemicals were obtained from Sigma (Deisenhofen, Germany) if not otherwise stated. Na_2ATP was purchased from Roche (Mannheim, Germany).

$P2X_7$ receptor expression in *X. laevis* oocytes

A plasmid encoding the human $P2X_7$ subunit (accession No. Y09561 (9)) was available for a previous study (11,23). Capped cRNA was synthesized from linearized templates with SP6 RNA polymerase (Epicentre Biotechnologies, Madison; WI), purified by Sepharose chromatography and phenol-chloroform extraction, dissolved in 5 mM Tris/HCl at pH 7.2 and adjusted to 0.5 μg/μl, using the optical density reading at 260 nm for quantitative analysis (OD 1.0 = 40 μg/μl).

Frogs were kept and subjected to surgical removal of part of their ovaries according to national guidelines on animal experimentation using tricaine methane sulfonate (MS-222, Sigma) for immersion anesthesia. After defolliculation by overnight incubation with collagenase (2 mg/ml; Worthington, Biochrom, Berlin, Germany), healthy stage V–VI oocytes were manually selected. $P2X_7$ subunit encoding cRNA was injected at ~0.1 μg/μl in 20 nl aliquots. The oocytes were maintained at 19°C in modified Barth solution (mM): 100 NaCl, 1 KCl, 1 $CaCl_2$, 1 $MgCl_2$, 5 HEPES supplemented with 10,000 U/ml of penicillin and 10 mg/ml streptomycin until used 1–3 days later.

Electrophysiology

All experiments were carried out at room temperature (≈22°C). Single channel currents were recorded from outside-out patches of the oocyte plasma membrane. Fast and reproducible solution exchange at the extracellular site of the patch was achieved by combining U-tube perfusion (24) with a piezo-driven liquid filament switch (25). The speed of solution exchange at the tip of the pipette was estimated by immersing the pipette in a 150 mM KCl bathing solution, and then shifting the pipette for 50 ms to a 100 mM NaCl solution supplied by the U-tube. From the exponential shift of the holding current, time constants of 0.6–0.8 ms were derived.

Microelectrodes were pulled from borosilicate glass, coated with Sylgard (Dow Corning, Midland, MI), and filled with a solution consisting of (in mM) 90 aspartic acid, 10 KCl, 10 EGTA, 10 BAPTA, 10 HEPES, and 0.5 $MgCl_2$, and pH 7.2 adjusted with KOH (K^+ pipette solution). The Cs^+ pipette solution had the same composition, except that KCl and KOH were replaced by CsCl and CsOH, respectively. In some initial experiments, pipette solutions were additionally supplemented with 5 mM MgATP. Patch pipettes had resistances between 6 and 15 MΩ as measured in an oocyte Ringer solution consisting of (in mM) 100 NaCl, 2.5 KCl, 1 $CaCl_2$, 1 $MgCl_2$, and 5 HEPES, with a pH of 7.4. Currents were recorded and filtered at 1 kHz (four-pole Bessel filter) using an Axopatch 1D patch-clamp amplifier (Axon Instruments, Foster City, CA) and sampled at 1 kHz (ensemble currents) or 5 kHz (single channel data). Current traces, each 400 ms in duration, were stored digitally and later analyzed on a personal computer using software programmed at our department (Superpatch 2000, SP-Analyzer by T. Böhm) and the computer program ASCD (generously provided by G. Droogmans, Catholic University Leuven, Belgium) based on least-square algorithms for fitting amplitude and dwell time histograms (26). For calculation of dwell time histograms, only apparent single channel patches (as judged by nonexistent overlapping openings at maximal open probabilities) were used. The minimum number of exponential terms required to describe the dwell time histograms was determined by minimizing the sum of weighted squared residuals.

The detection threshold for opening and closing was set at 50% of the single channel current amplitude. Correlations between adjacent open and shut times were calculated and tested for significance according to Colquhoun and Sakmann (27).

For patch-clamping, the vitelline layer was removed with fine forceps after a brief exposure of the oocyte to a hypertonic medium. To establish the outside-out configuration, an oocyte was placed in a small chamber perfused with oocyte Ringer solution. The pipette with the outside-out membrane patch was then transferred to another chamber, which was perfused with a bathing solution containing (in mM) 100 NaCl, 0.5 $CaCl_2$, 5 HEPES, pH 7.4. The liquid filament solution flowing out of the U-tube (U-tube solution) additionally contained free ATP^{4-} in concentrations indicated in the figures and in the text. The total concentrations of ATP and $CaCl_2$ were adjusted in such a way that the free Ca^{2+} concentration was kept constant at 0.5 mM (28). The total concentrations of Ca^{2+} and ATP used to adjust the concentrations of ATP^{4-} indicated in the figures are included as Supplementary Material S1.

If not otherwise indicated, averaged data are given as mean ± SD of measurements in N patches. The statistical significance ($P < 0.05$) of differences between means was determined by one-way ANOVA followed by a Bonferroni multiple comparison t-test using Jandel Sigmastat statistical software (SPSS, Chicago, IL). The Sigmaplot program (SPSS) was used for nonlinear function fitting and graphical presentation of the data. Theoretical values of dwell times, open probabilities, and relaxation time constants were calculated according to (29) using the freely accessible program SCALCS (http://www.ucl.ac.uk/Pharmacology/dc.html).

RESULTS

Different components of ATP-induced patch currents

Fig. 1 *A* shows a typical example of outside-out patch currents before, during, and after extracellular exposure to ATP^{4-}. The membrane patch was excised from an oocyte injected with cRNA for the human $P2X_7$ subunit one day earlier. Two current components are evident. One component consists of inward single channel current events (Fig. 1 *B*) with a single channel current amplitude of −1.3 pA (Fig. 1 *C*). Single channel openings were observed shortly after ATP^{4-} application and disappeared immediately after commencing ATP^{4-} washout. The single channel current amplitude, as well as the open probability, did not obviously change during ATP^{4-} applications during a time period of several minutes. Furthermore, the use of pipette solutions supplemented with MgATP (see Materials and Methods) did not significantly change the amplitude and kinetics of $P2X_7$ receptor-dependent single channel currents (results not shown).

The second component is a smooth inward shift of the holding current with an approximately exponential time course of activation and deactivation during ATP^{4-} application and withdrawal, respectively. Similar currents were also seen in patches from $P2X_7$ subunit cRNA-injected oocytes without single channel openings (Fig. 1 *D*) ($N = 60$),

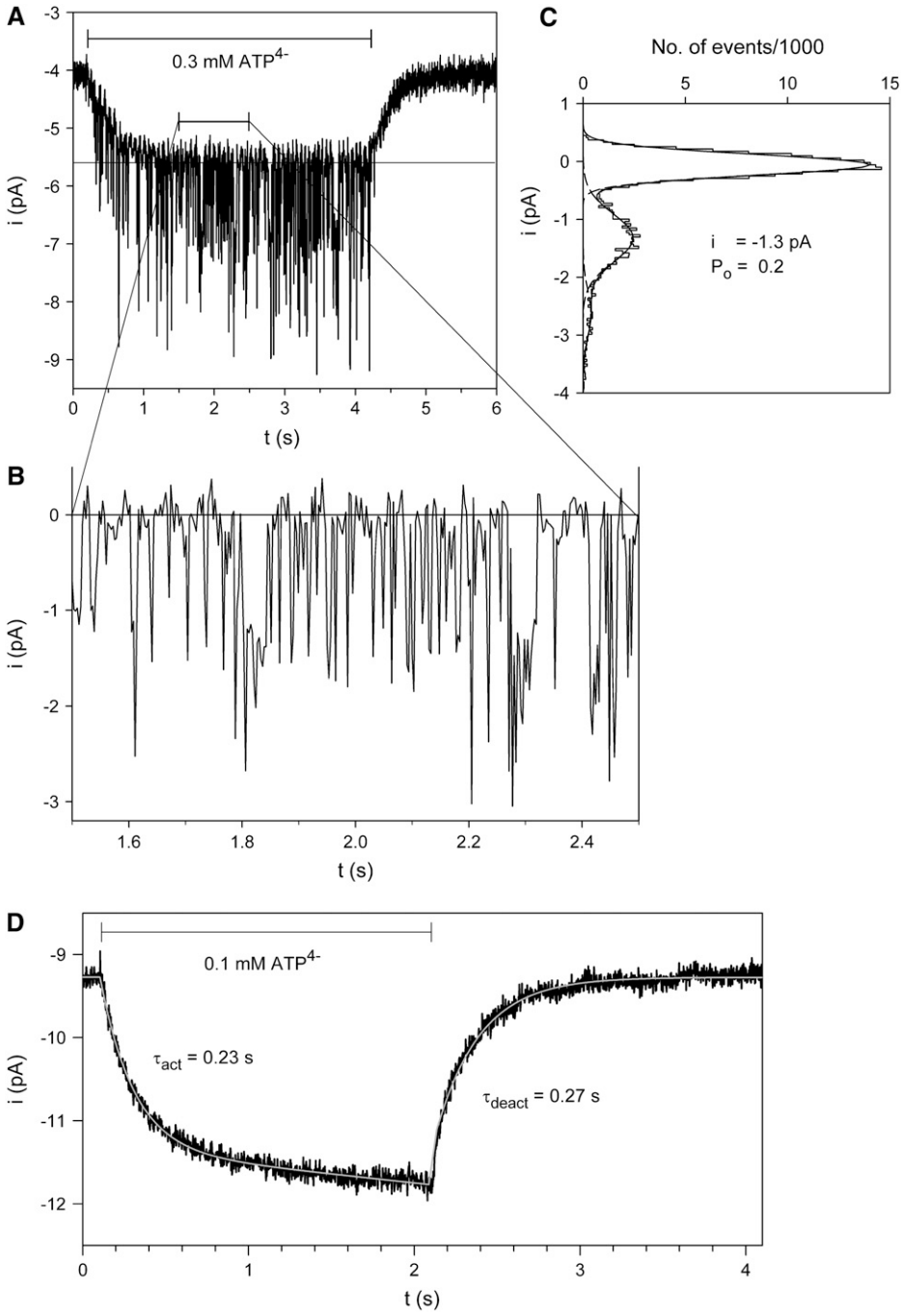

FIGURE 1 ATP-dependent membrane patch currents. (*A*) Representative current trace evoked by ATP^{4-} from an outside-out membrane patch as indicated. (*B*) Single channel events from *A* are shown on an extended timescale. (*C*) Amplitude histogram of the single channel currents from panel *A* in the time window from 1.3 to 4.2 s after subtraction of the smooth current component. Data were fitted by the sum (*solid line*) of three Gaussian curves (*dashed lines*). (*D*) Typical time course of ATP-evoked current of a patch without visible single channel events. The activating and deactivating currents were fitted (*white line*) according to Eqs. 1 and 2, respectively. $V_h = -120$ mV; Cs^+ pipette solution was used.

from oocytes injected with H_2O only ($N = 5$), and from non-injected oocytes ($N = 8$, data not shown). ADP^{3-}, UTP^{4-}, and GTP^{4-} also elicited the smooth current component, but did not induce single channel openings in concentrations up to 1 mM (data not shown) in patches with clear single channel activity in response to 0.1 mM ATP^{4-} ($N = 5$).

For quantitative analysis of current activation kinetics, the activating part of this ''smooth'' current component ($i_{act}(t)$) was fitted to

$$i_{act}(t) = i_{act,\infty} \times \left(1 - e^{-\frac{t-t_{del,act}}{\tau_{act}}}\right) + s \times (t - t_{del,act}) + i_0, \quad (1)$$

where $t_{del,act}$ is the delay of the onset of the ATP^{4-}-induced current, $i_{act,\infty}$ is the amplitude of the theoretical steady-state plateau current after infinite time of ATP^{4-} application, τ_{act} is the activation time constant, s is the slope of the linearly increasing current, and i_0 is the steady-state current in the absence of ATP^{4-}.

The deactivating part of the smooth current component ($i_{deact}(t)$) during washout of ATP^{4-} was approximated by

$$i_{deact}(t) = i_{deact} \times e^{-\frac{t-t_{del,deact}}{\tau_{deact}}} + i_0, \quad (2)$$

where i_0 has the same meaning as in Eq. 1, $t_{del,deact}$ is the delay of deactivation of the ATP^{4-}-induced current, i_{deact} is the initial amplitude, and τ_{deact} is the time constant of the deactivating component, respectively. To allow the smooth current component to be properly distinguished from the single channel component, especially in multichannel patches, the kinetics and ATP^{4-} dependence of the smooth current component were investigated in more detail. Time constants of activation and deactivation of ~400 ms were derived that were independent of the ATP^{4-} concentration (Fig. 2 *A*). The linearly increasing (Fig. 2 *B*) as well as the exponentially activating (Fig. 2 *C*) current component increased with the applied ATP^{4-} concentration without displaying saturation. The amplitude of the exponentially rising component was additionally dependent on the leak current before ATP^{4-} application (Fig. 2 *D*). This, together with the occurrence of a similar smooth current component in water- and noninjected oocytes as well as upon application of ADP^{3-}, UTP^{4-}, or GTP^{4-} (see above), suggests that ATP^{4-} exerts a nonspecific effect on the seal between the patch membrane and the pipette. Alternatively, another leak-determining conductance of the patch may be nonspecifically increased by ATP^{4-}. For evaluation of $P2X_7$ receptor-dependent single channel kinetics, measurements of single channel current amplitudes or dwell times started 1 s after application of ATP^{4-} and the steady state or slowly increasing components of the smooth current component were subtracted by the software used.

In some patches, ATP^{4-}-induced channel openings with long open times of ~20 ms were observed. The probability of the occurrence of these opening events increased with increasing ATP^{4-} concentrations (Fig. 3 *C*) and with longer or repeated ATP^{4-} applications (Fig. 3 *A*). In contrast to the short channel openings (described in detail below), the single channel events with long duration deactivated slowly after ATP^{4-} withdrawal. The absence of overlapping long and short single channel currents suggests that the same channel exists in two different gating modes in the same patch. To address the question of whether the long openings are in any way related to the phenomenon of ATP^{4-}-induced pore dilatation observed in macroscopic recordings (21), we assessed the permeability of single $hP2X_7$ receptor channels to the organic cation $Tris^+$. We expected dilatation of the $hP2X_7$ channel pore to be reflected by a time-dependent increase in the permeability of $Tris^+$ (diameter ~7 Å) during sustained activation by ATP, as has been observed under macroscopic conditions for even larger cations such as *N*-methyl-D-glucamine ($NMDG^+$, diameter ~9 Å). The single channel patch recording shown in Fig. 3 *B* was selected to show both short and long openings in Na^+-based media. Fig. 3 *B* shows that only very small single channel inward currents could be recorded after exchange of equimolar $Tris^+$ for external Na^+. Low permeability to $Tris^+$ is also apparent from the very negative reversal potential. Moreover, the current amplitude did not increase in magnitude during 20 s of sustained ATP^{4-} activation (Fig. 3 *B*) at a holding potential (V_h) as negative as −110 mV, and the reversal potential did not shift to less negative values. This indicates that the very low permeability of the ATP^{4-}-opened $hP2X_7$ receptor to $Tris^+$ did not increase with time.

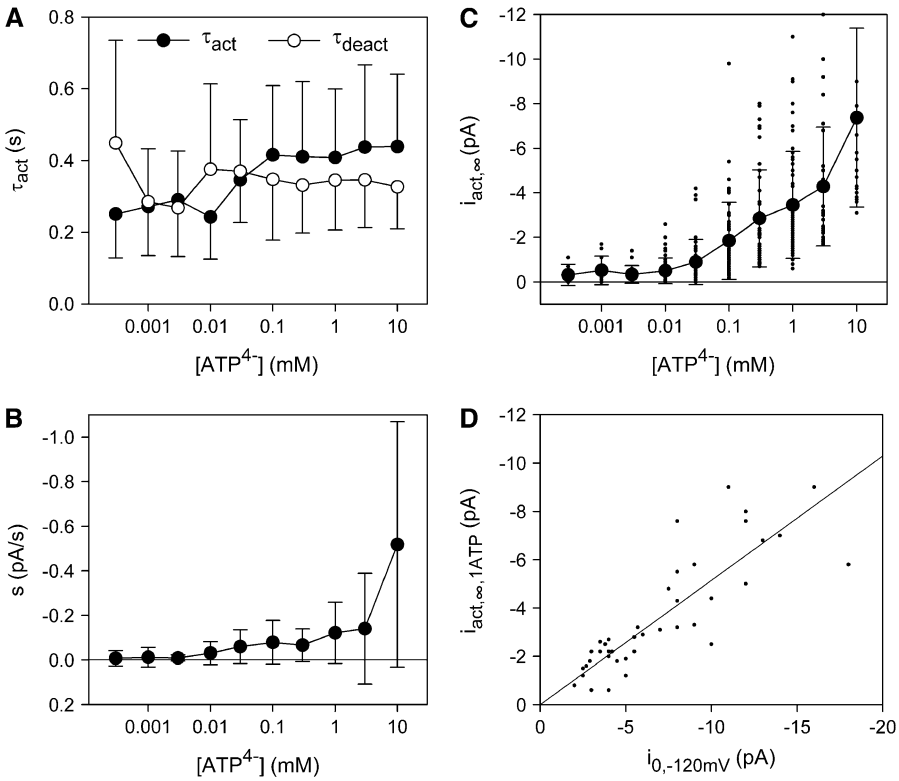

FIGURE 2 Analysis of the ATP-induced smooth patch current component. ATP^{4-} dependence of activation and deactivation time constants (*A*), the linearly activating component *s* (*B*), and the amplitude of the activating current (*C*). (*D*) Dependence of the exponentially activating current amplitude $i_{act,\infty}$ evoked by 1 mM ATP^{4-} on the current before ATP application. V_h = −120 mV, N = 5–20 patches from 20 different oocytes.

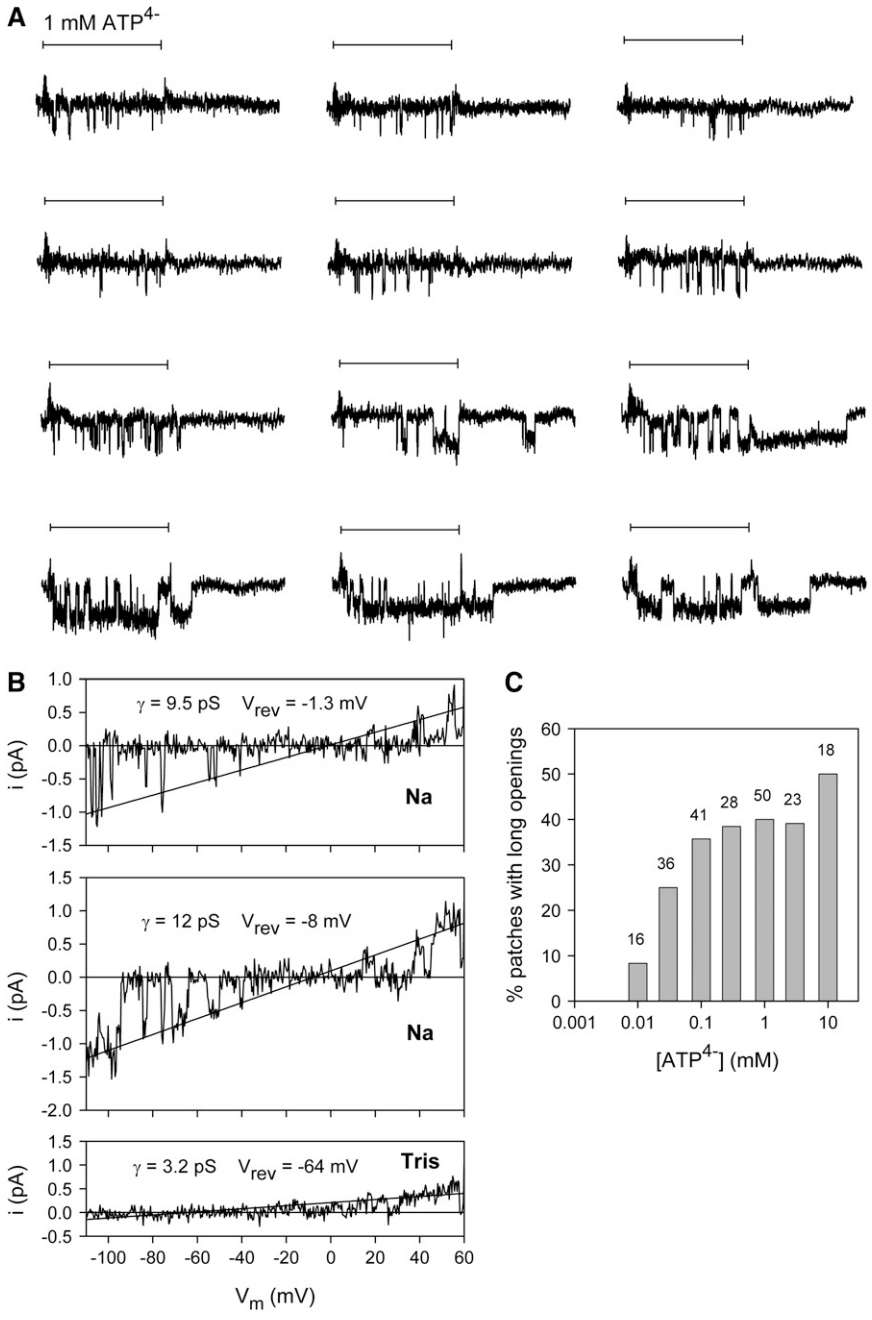

FIGURE 3 Long-lasting P2X$_7$ channel openings. (*A*) Typical current traces (after subtraction of the smooth component) evoked by repeated ATP^{4-} applications (indicated by *horizontal bars*) in 4 s intervals. K^+ pipette solution, V_h −120 mV. (*B*) Typical single channel recording during voltage ramp pulses extending from −120 to +60 mV during hP2X$_7$ receptor activation by 1 mM ATP^{4-}. The smooth current component was subtracted. The top and middle records show typical traces with short openings and long openings, respectively, in Na^+-based extracellular solution. Bottom record shows typical traces of the same patch after replacement of Na^+ by equimolar $Tris^+$. No obvious single channel current changes were observed during a 20 s application of 1 mM ATP^{4-}. The indicated slope conductances γ and reversal potentials V_{rev} were calculated by linear regression fitting (shown as *straight lines*) of the voltage dependence of the open channel currents. (*C*) Dependence of the probability to measure long single channel openings on the activating $[ATP^{4-}]$; $N = 16$–50 patches from 10 to 35 different oocytes. Numbers above columns indicate N.

Fig. 4 *A* demonstrates a patch current record with coexisting occurrence of short and long-lasting channel openings. The amplitude histogram (Fig. 4 *B*) reveals different single channel amplitudes of −1.3 pA and −2.0 pA. The closed times (Fig. 4 *E*) were not obviously different from that obtained from patches with short openings only (see Fig. 7 *D*). Compared to recordings with only short openings, the open time histogram (Fig. 4 *D*) shows an additional third dwell time component with a mean open time of 24 ms.

An analysis separating short (<9 ms) and long (>9 ms) openings according to the open time histogram disclosed that the short openings had the smaller single channel current amplitude. The results of similar measurements carried out at different V_h are depicted in Fig. 4 *C* and identified slope conductances of 9.5 pS and 14.8 pS for the short and long openings, respectively. To allow for statistical analysis, a larger dataset was generated by applying the same threshold criterion of 9 ms open time to the analysis of additional single channel patches. Conductances were determined by fitting the current-voltage relation in the V_h range between −80 and 0 mV. The conductances of short channel openings (9.2 ± 0.6 pS, mean ± SE, $N = 48$) and long channel openings (13.1 ± 0.9 pS, $N = 23$) were significantly different. The mean closed times, however, were not significantly different between

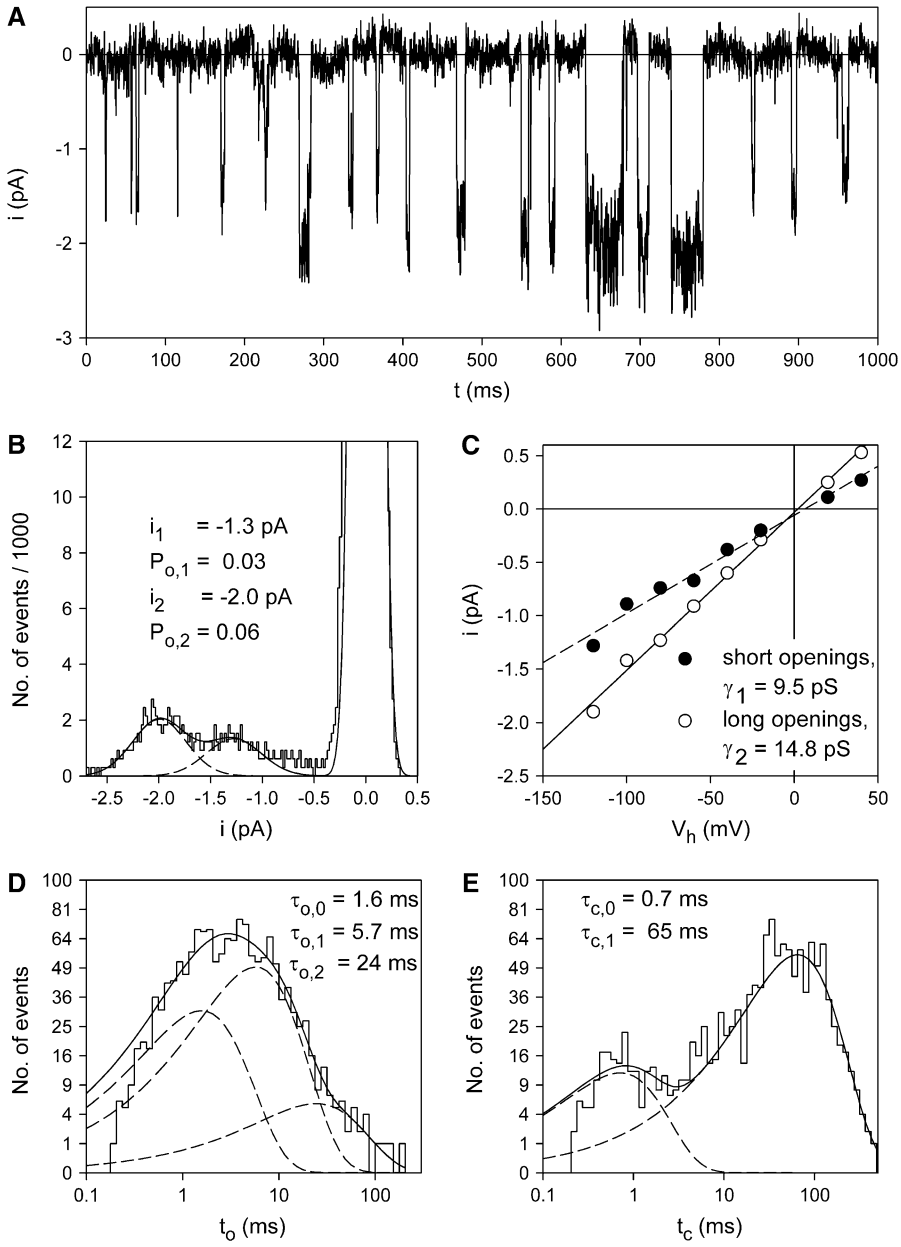

FIGURE 4 Two gating modes of $P2X_7$ channels. (*A*) Typical recording of ATP^{4-}-induced coexisting short and long-lasting openings of single $P2X_7$ channels. K^+ pipette solution, $V_h = -120$ mV, $[ATP^{4-}] = 0.1$ mM. (*B*) Amplitude histogram of the patch currents shown in *A*. (*C*) Voltage dependence of the amplitudes of long- and short-lived single channel opening events, which were obtained from amplitude histograms as shown in panel *B*. Slope conductances were calculated by linear regression from -100 to $+40$ mV ($r > 0.98$). Open (*D*) and closed time histograms (*E*) of the patch currents shown in *A* were fitted by the sum (*solid line*) of three and two exponential functions (*dashed lines*), respectively. The threshold for detection of openings and closings was set to -0.65 pA.

patches displaying either only short openings (23 ± 4 ms, $N = 21$) or both short and long openings (22 ± 8 ms, $N = 10$) upon activation by 1 mM ATP^{4-}.

The occurrence of long openings appeared to depend, in an unpredictable way, on the particular oocyte preparation. Approximately 30% of oocytes did not display long-lasting openings despite the application of high ATP^{4-} concentrations for up to 10 min, whereas patches from other oocyte preparations were dominated by long-lasting openings.

ATP^{4-} dependence of $P2X_7$ receptor channels

Fig. 5 shows an example of ATP^{4-}-dependent channel gating in a patch with obviously only short-lasting channel openings. Channel openings were induced by a minimum concentration of 10 μM ATP^{4-}. The open probability increased with increasing $[ATP^{4-}]$ and was almost saturated at 1 mM ATP^{4-}. The single channel current amplitude was not obviously altered by increasing $[ATP^{4-}]$. This is substantiated by the corresponding amplitude histograms, which also demonstrate an increased closed channel noise at high $[ATP^{4-}]$. The simplest interpretation is a destabilizing effect of high ATP^{4-} concentrations on the patch seal.

Fig. 6 demonstrates the stability of the measured open and shut times. For patches without long openings, significant correlations were found only occasionally for open times (3 of 42 patches, mean over all patches 0.02 ± 0.08) as well as for closed times (8 of 42 patches, mean over all patches 0.07 ± 0.11) both at low and high $[ATP^{4-}]$. In contrast, patches

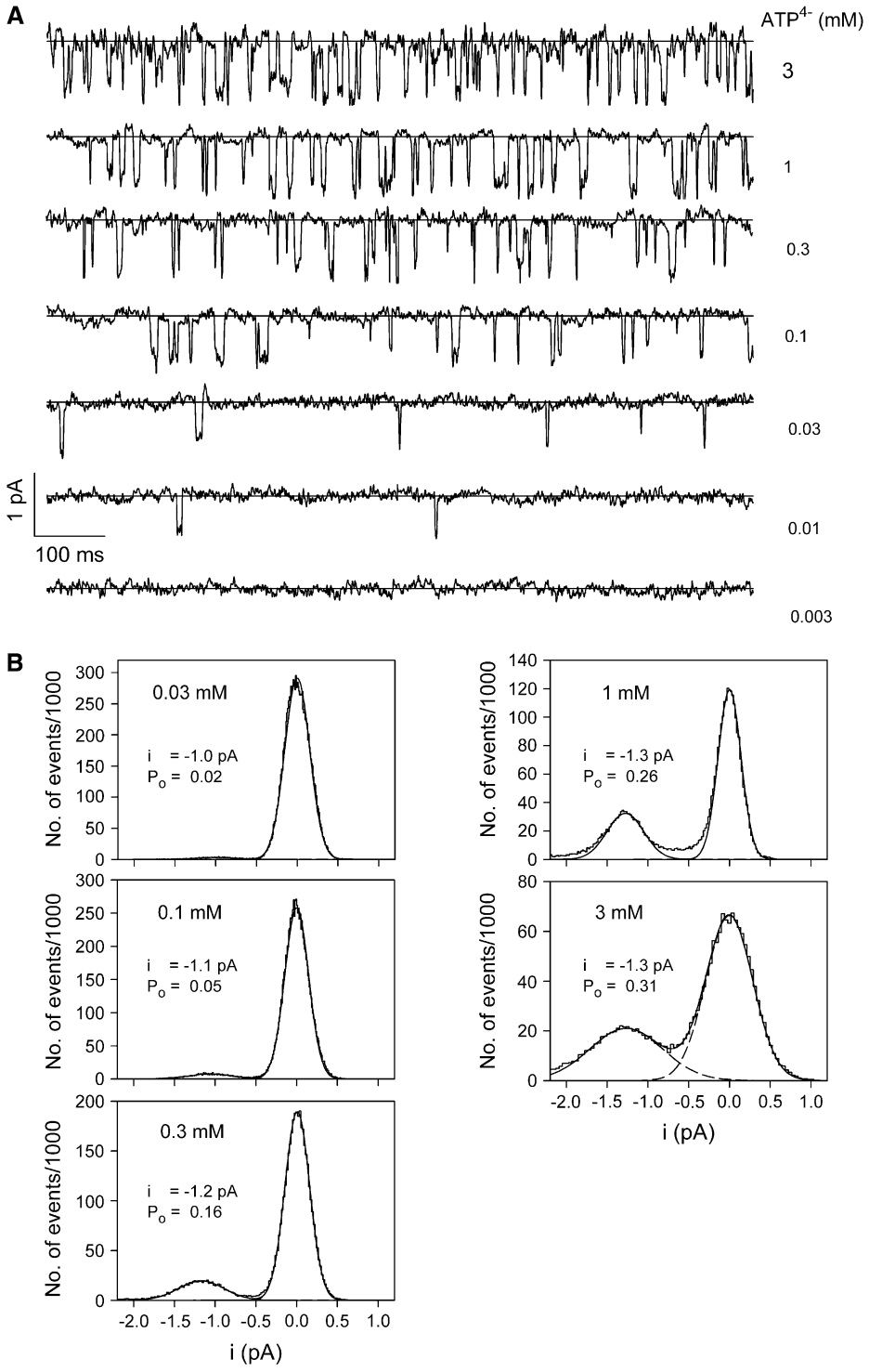

FIGURE 5 Typical examples of ATP^{4-}-dependent single P2X$_7$ channel gating. (*A*) Channel currents were induced by the indicated ATP^{4-} concentration. The straight lines specify the closed channel current as obtained by subtraction of the smooth current component. (*B*) Corresponding amplitude histograms. $V_h = -120$ mV, K^+ pipette solution.

with long openings in the dwell time histogram more often displayed significant correlations (open times: 15 of 18 patches, mean over all patches 0.20 ± 0.11; closed times: 10 of 18 patches, mean 0.14 ± 0.12).

Fig. 7 summarizes the ATP dependence of P2X$_7$ receptor channels. The single channel current amplitudes were not significantly [ATP^{4-}]-dependent (Fig. 7 *A*).

Channel open probabilities (P_o) were calculated from the amplitude histogram. Only patches with no more than three overlapping single channel events were used. The number of channels in a patch was assumed to correspond to the maximal number of overlapping events at an activating ATP^{4-} concentration of 1 mM, at which P_o is high. In cases of more than one active channel in the patch, an equal P_o for all these

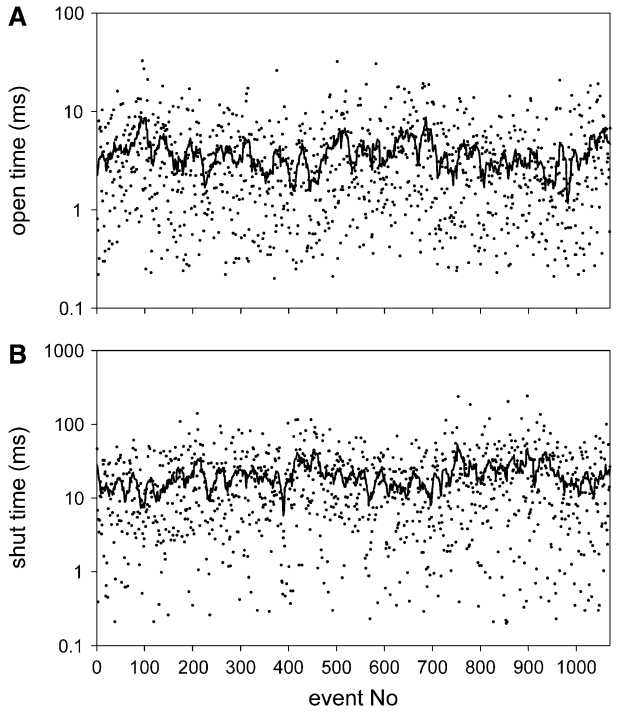

FIGURE 6 Stability of single channel dwell times. Typical stability plot for a record without prominent long openings. The plots are from the data shown in Fig. 5 ([ATP^{4-}] = 0.3 mM). The overlay demonstrates a running average of 15 values each.

channels was assumed, and the mean P_o was calculated by the binomial distribution,

$$P_o = 1 - \sqrt[n]{P(0)}, \tag{3}$$

where n is the number of active channels in the patch and $P(0)$ is the closed probability derived from the fit of the amplitude histogram. The open probabilities of the short and long openings were voltage-independent at negative V_h in the range of −160 to −0 mV (data not shown).

In the simplest case, when all the ATP^{4-} binding sites have the same affinity and there is no cooperative interaction between them, the [ATP^{4-}] dependence of the open probability of the short and the long openings is given by

$$P_o([ATP^{4-}]) = \frac{P_{o,\infty}}{\left(1 + \frac{10^{-\log K_d}}{[ATP^{4-}]}\right)^n}, \tag{4}$$

where $P_{o,\infty}$ is the maximal open probability at ATP^{4-} concentrations saturating the agonist binding sites with the apparent dissociation constant K_d. Approximations yielded (mean ± SE) maximal open probabilities of 0.26 ± 0.02 and 0.30 ± 0.02, pK_d values of −3.60 ± 0.11 and −3.93 ± 0.14, and n values of 1.4 ± 0.3 and 1.1 ± 0.4 and for the short and long-lasting openings, respectively. All approximated values were not significantly different for the short and the long-lasting openings (Fig. 7 *B*).

The [ATP^{4-}]-dependence of the dwell times are depicted in Fig. 7, *C* and *D*. Occasionally, some ultra-short openings and closings (with mean dwell times at ~0.8 ms) occurred mainly at high [ATP^{4-}] and positive membrane voltages (data not shown), where the current noise was most likely enlarged due to destabilization of the patch. Under these conditions, the survival time of the patches was decreased accordingly. This suggests that the ultra-short events reflect current noise rather than real channel states. The short mean open times stayed nearly constant, whereas the long closed times became shorter at increasing [ATP^{4-}].

The increased P_o at higher [ATP^{4-}] results from a decreased mean closed time of the long-lasting closings, because indications for a change of the number of activated channels at different [ATP^{4-}] or changes of the mean open time (Fig. 7 *C*) were not obtained. Furthermore, increasing [ATP^{4-}] from 0.03 to 3 mM increased the open probability of the short openings by tenfold (from 0.03 to 0.28), and led to a ~10 % decrease of the long-lasting closings (from 147 to 14 ms).

The large standard deviations indicate a high scattering of the open probabilities, which, according to our experience, results largely from variable open probabilities at the same [ATP^{4-}] of different oocytes. This variability seems to be a characteristic of the particular oocyte preparation rather than of different oocytes of the same preparation, different patches from the same oocyte, or time-dependent changes of the P_o of channels in the same patch. Some support for this view can be derived from the larger relative variance SD/mean of the absolute open probability P_o at 0.3 mM ATP^{4-} than that of the relative open probability $P_{o,rel}$ related to P_o at 1 mM ATP^{4-} in the same patch ($P_{o,rel} = P_o/P_o$(1 mM ATP^{4-})), which were calculated to be 0.57 and 0.49, respectively.

Activation and deactivation kinetics

The activation and deactivation kinetics were studied by using an ultra-fast solution exchange system (see Materials and Methods). To obtain global activation and deactivation time courses of $P2X_7$ receptors at certain ATP^{4-} concentrations, either multichannel patches were used or patch current measurements of repeated ATP^{4-} applications were averaged. Because slowly deactivating long-lasting openings occurred infrequently, only patches without such events were analyzed. Fig. 8 shows typical current traces of a multichannel patch. The activation time course was approximated by

$$i_{act}(t) = i_{act,\infty,1} \times \left(1 - e^{-\frac{t - t_{del,act}}{\tau_{act,1}}}\right) + i_{act,\infty,2} \times \left(1 - e^{-\frac{t - t_{del,act}}{\tau_{act,2}}}\right) + s \times (t - t_{del,act}) + i_0, \tag{5}$$

where $i_{act,\infty,1}$ and $i_{act,\infty,2}$ are the amplitudes of steady-state currents after infinite time of ATP application, and $\tau_{act,1}$ and

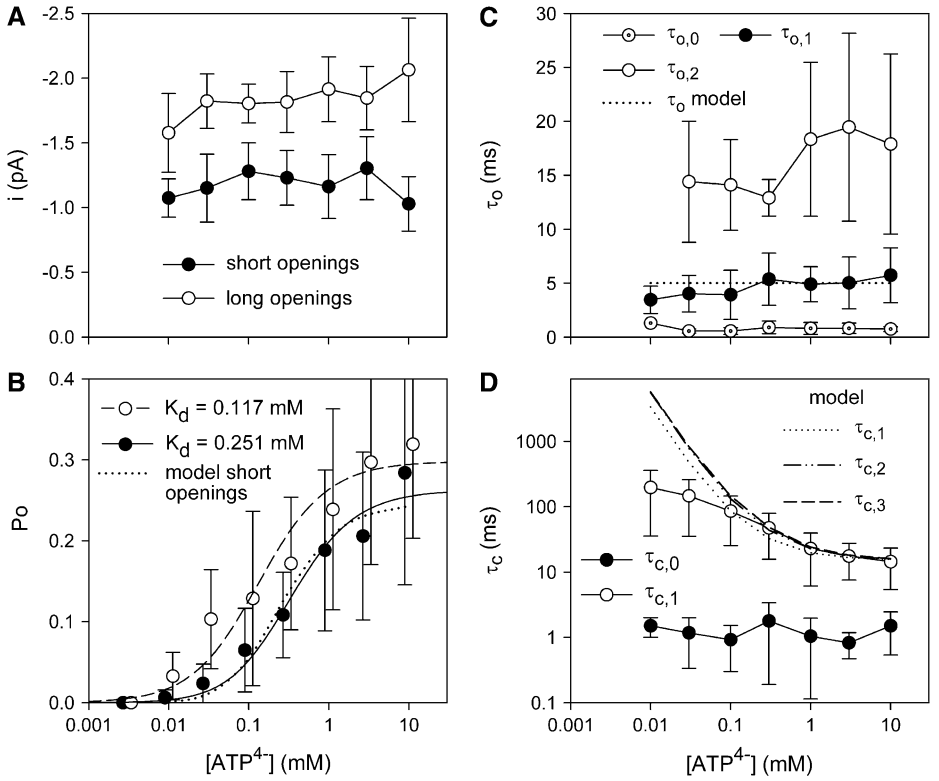

FIGURE 7 ATP^{4-}-dependence of P2X$_7$ channel gating. (*A*) Dependence of single channel current amplitude of short (<9 ms, *solid circles*) and long (>9 ms, *open circles*) channel openings. Means for both gating modes are significantly different, but independent of [ATP^{4-}]. (*B*) Open probability calculated from amplitude histograms. Data were fitted by Eq. 4. P_o([ATP^{4-}]) of the short openings as calculated by the C-C-C-O model (see Fig. 9 *C*) is depicted as a dotted line. (*C*, *D*) Mean open and closed time components measured as shown in Fig. 4. All mean open time components and the short mean closed times ($\tau_{c,0}$) were independent of [ATP^{4-}]. The open and closed times predicted by the model are drawn as dotted and dashed lines as depicted in the inset. N = 3–18 patches from 3 to 13 different oocytes, K^+ pipette solution, V_h = −120 mV.

$\tau_{act,2}$ are the activation time constants of the slow and fast activating current components, respectively. The values s, $t_{del,act}$, and i_0 have the same meaning as in Eq. 1. The deactivation during fast ATP^{4-} washout was described by

$$i_{deact}(t) = i_{deact,1} \times e^{-\frac{t-t_{del,deact}}{\tau_{deact,1}}} + i_{deact,2} \times e^{-\frac{t-t_{del,deact}}{\tau_{deact,2}}} + i_0, \quad (6)$$

where i_0 and $t_{del,deact}$ have the same meaning as in Eq. 2, $i_{deact,1}$ and $i_{deact,2}$ are the initial amplitudes, and $\tau_{deact,1}$ and $\tau_{deact,2}$ are the time constants of the slow and fast deactivating components, respectively.

The fast activating and deactivating components ($i_{act,\infty,2}$ and $i_{deact,2}$ with the corresponding time constants $\tau_{act,2}$ and $\tau_{deact,2}$) describe the activation and deactivation of the ATP-dependent single channel events. The time courses of the slow activating and deactivating components described here correspond to activation and deactivation kinetics of the smooth current components measured in patches without channel openings, which most likely reflect the effect of ATP^{4-} on the seal leak (see above). According to the ATP^{4-} dependence of the smooth current component (Fig. 2, *B* and *C*), the slow activating and deactivating components here were prominent only at high [ATP^{4-}]. This can be directly seen by comparing the current traces at 0.1 and 1 mM ATP^{4-} in Fig. 8. So far, the nature of a slowly deactivating current component upon washout of low [ATP^{4-}] is unexplained (see effect of 0.01 mM ATP^{4-} in Fig. 8).

The dependence of the fast rising and decaying components, reflecting single channel activation and deactivation, on membrane voltage and activating [ATP^{4-}] was investigated in more detail (Fig. 9). Activation and deactivation of P2X$_7$ receptors were virtually voltage-independent at negative membrane potentials of −160 to −40 mV (data not shown). The deactivation time course was largely independent of [ATP^{4-}] (Fig. 9 *B*). Surprisingly, the activation time course was not much accelerated by increasing the activating [ATP^{4-}] (Figs. 8 and 9 *A*). If the binding of ATP^{4-} is the rate-limiting step for channel opening, the activation rate constant should increase proportional to the activating [ATP^{4-}]. However, a 300-fold increase of [ATP^{4-}] increased the rate constant of channel activation (R_{act} = 1/$\tau_{act,2}$) less than twofold, from 1/24 ms to 1/14 ms (Fig. 9 *A*). This suggests that the opening of P2X$_7$ channels is rate-limited by a conformational change of the receptor after ATP^{4-} binding (see the model below).

A model describing the kinetics of P2X$_7$ receptor-mediated currents

We were looking for a model describing the microscopic (dwell times) as well as the macroscopic (current relaxation during activation and deactivation) kinetic behavior of P2X$_7$ receptor-mediated currents. The simplest model for a ligand-gated ion channel is one with one closed and one open state, C and O, respectively. To describe the shallow dependence of the macroscopic activation time course on [ATP^{4-}], we first adapted the rate constants of a two-step kinetic model

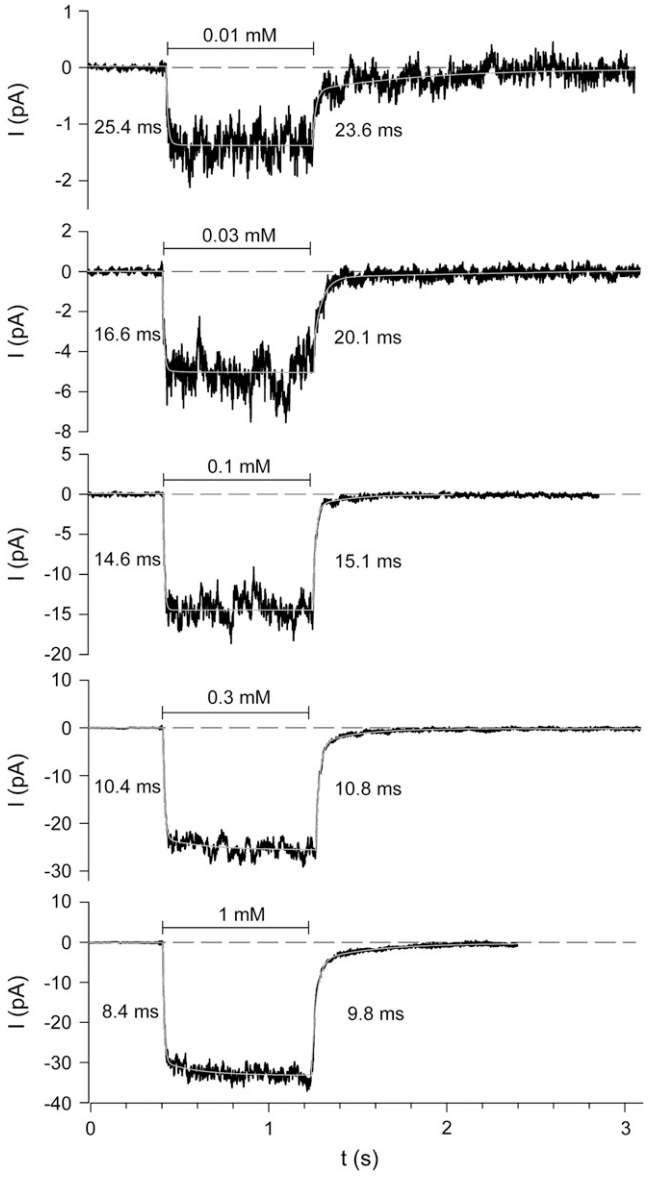

FIGURE 8 Examples of activation and deactivation kinetics of $P2X_7$ receptors. Mean currents (*solid lines*) of 3–12 repeated ATP^{4-} applications of indicated concentrations. Dashed lines mark the current level before agonist application. The white lines represent the approximation of the activation and deactivation time course according to Eqs. 5 and 6, respectively. The calculated time constants of fast activation and deactivation are shown at the left and right site of the ATP^{4-}-induced current, respectively. K^+ pipette solution, $V_h = -120$ mV.

with two closed states, C_1 and C_2, and one open state O (29). According to this model, agonist binding and channel opening occur with distinct rate constants, thus accounting for a presumably rate-limiting opening step:

$$C_1 \underset{k_{-1}}{\overset{k_{+1}\cdot[ATP^{4-}]}{\rightleftharpoons}} C_2 \underset{\alpha}{\overset{\beta}{\rightleftharpoons}} O. \tag{7}$$

The values k_{+1} and k_{-1} describe the rates of ATP^{4-} binding and dissociation, and β and α are the rate constants for channel opening and closing, respectively. The following constraints were imposed. First, α was set to 200 s^{-1} to obtain mean open times of 5 ms (Fig. 7 *C*) since $\tau_o = 1/\alpha$ (29). Second, $\beta = 66$ s^{-1} was chosen to model a maximal open probability of 0.25 (Fig. 7 *B*). Finally, k_{-1} and k_{+1} were set to 50 s^{-1} and 360 mM^{-1} s^{-1} to model the mean closed time at 0.3 mM ATP^{4-} and an EC_{50} of ~0.3 mM ATP^{4-}, respectively. The effect of choosing these rate constants on the microscopic and macroscopic kinetic behavior was checked using the program SCALCS (see Materials and Methods). The C-C-O model described the ATP^{4-} dependence of the dwell times, the open probability, and the activation time course sufficiently well, but the deactivation time constants derived from the model were too large. Therefore, we extended the model to include a second independent ATP^{4-} binding step connected to the closed state, assuming the same affinity of two binding sites. C_1, C_2, and C_3 therefore represent unliganded, monoliganded, and biliganded closed states:

$$C_1 \underset{k_{-1}}{\overset{2\cdot k_{+1}\cdot[ATP^{4-}]}{\rightleftharpoons}} C_2 \underset{2\cdot k_{-1}}{\overset{k_{+1}\cdot[ATP^{4-}]}{\rightleftharpoons}} C_3 \underset{\alpha}{\overset{\beta}{\rightleftharpoons}} O. \tag{8}$$

Using the fitted kinetics parameters, the dotted and dashed lines in Figs. 7 and 9 were calculated from the C-C-C-O model. This model predicts three different mean closed times (Fig. 7 *D*), which, however, are so similar that the scattering of the data did not allow them to be resolved in the dwell time histograms. Furthermore, although the model predicts three time constants of macroscopic activation and of deactivation, one of these time constants is so prominent that the activation and deactivation time courses could both be well approximated by single exponential functions (Eqs. 9 and 10) (Fig. 9 *C*). The other time constants mainly give rise to delays, which could not be resolved in our noisy measurements. To compare the measured time constants with predictions of our model, we fitted the modeled currents by the following monoexponential activation and deactivation time courses (Fig. 9 *C*),

$$P_{o,act,model}(t) = P_{o,\infty} \times \left(1 - e^{-\frac{t - t_{del,act}}{\tau_{act,2,model}}}\right), \tag{9}$$

$$P_{o,deact,model}(t) = P_{o,\infty} \times e^{-\frac{t - t_{del,deact}}{\tau_{deact,2,model}}}, \tag{10}$$

where $P_{o,\infty}$ is the channel open probability after infinitely long ATP^{4-} application, and $\tau_{act,2,model}$ and $\tau_{deact,2,model}$ are the time constants of activation and deactivation of $P2X_7$ receptor-mediated currents. The ATP^{4-} dependence of these time constants is depicted in Fig. 9, *A* and *B*.

Single channel kinetics in the oocyte-attached configuration

To analyze the possible influence of diffusible intracellular molecules on single channel kinetics, we recorded ATP^{4-}-induced

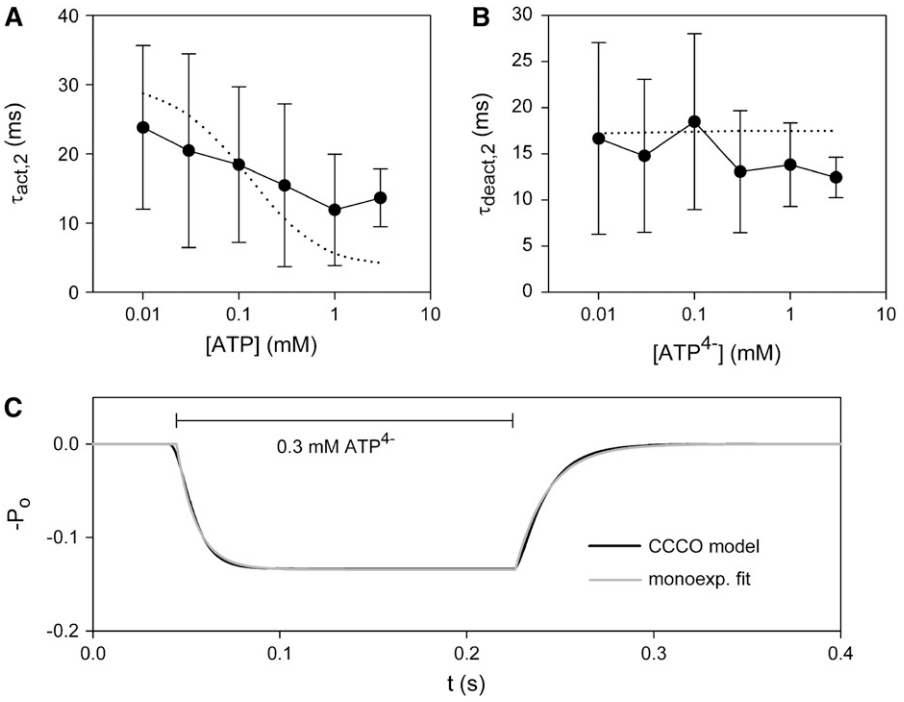

FIGURE 9 Dependence of activation and deactivation of P2X$_7$ receptors on agonist concentration. (*A*, *B*) The mean time constants ± SD for fast activation and deactivation correspond to the approximations of Fig. 8. (*Dotted lines*) [ATP^{4-}] dependences of the time constants predicted by the C-C-C-O model (Eq. 8). (*C*) The time course of activation and deactivation of P2X$_7$-dependent channels as predicted by the C-C-C-O model (Eq. 8) was fitted by monoexponentially relaxing functions (Eqs. 9 and 10).

currents in the cell-attached mode from P2X$_7$ receptor-expressing oocytes with pipette solutions containing either 0.1 or 0.3 mM ATP^{4-}. Because extracellular wash-in and wash-out of ATP^{4-} was not possible in this configuration, P2X$_7$ receptor-mediated currents were identified using the voltage dependence of the characteristic single channel parameters. Fig. 10 shows a typical example of such a patch-clamp recording (out of $N = 5$) without overlapping single channel events as an indication for only one functional P2X$_7$ receptor channel in the patch. The values measured for conductance, open probability, and dwell times of single channel currents were well within the range covered by one standard deviation of the analogous values measured in the outside-out configuration. The single channel characteristics did not change for the 20 min during which the patch remained intact. P2X$_7$-like single channel currents were never observed in cell-attached recordings with ATP-free pipette solutions. From recordings at a total of five cell-attached patches with 0.1 mM ATP^{4-} in the pipette, mean open and closed times of 3.9 ± 2.3 ms and 44 ± 12 ms were calculated, respectively. These values are not significantly different from the values obtained in the outside-out configuration (see Fig. 7, *C* and *D*).

DISCUSSION

Dissecting different ATP-induced patch currents of P2X$_7$ receptor-expressing oocytes

The present single channel measurements allow us to confine ATP^{4-}-induced currents reliably to a homogenous population of single channel events characterized by a defined single channel conductance and mean open time. The currents described here were the only single channel events that could be activated rapidly and repeatedly by ATP^{4-}. Other single channel events occurred infrequently and were only loosely coupled to ATP^{4-} application or withdrawal. This, together with the finding that these ion channel activities occurred only in membrane patches from P2X$_7$ receptor-expressing oocytes, ensures that P2X$_7$ receptor-mediated currents were recorded rather than other secondarily evoked currents.

In the present patch-clamp experiments, an additional current component was persistently observed, which did not show resolvable single channel events (Figs. 1 and 2). Most likely, this current component results from an unspecific effect of negatively charged purines on the seal leak, because it 1), was independent of P2X$_7$ receptor expression; 2), did not show a saturating dependence on [ATP^{4-}]; 3), did not change its time course with [ATP^{4-}]; 4), was also observed at 1 mM ADP^{3-}, UTP^{4-}, or GTP^{4-}, which did not evoke single channel currents; and 5), was related in magnitude to the leak current recorded before ATP^{4-} application, i.e., the seal resistance. An ATP-induced shift of the holding current had already been observed in measurements of native P2Z receptor-dependent single channel currents, which almost certainly represent P2X$_7$ receptor-mediated currents (30). The smooth current component must be taken into account in the analysis of quasimacroscopic currents obtained from multichannel patches or averaged single channel records when single channel events become hardly visible. We used this type of measurement mainly for analyzing the macroscopic kinetics of P2X$_7$ receptor-mediated currents. Fortunately,

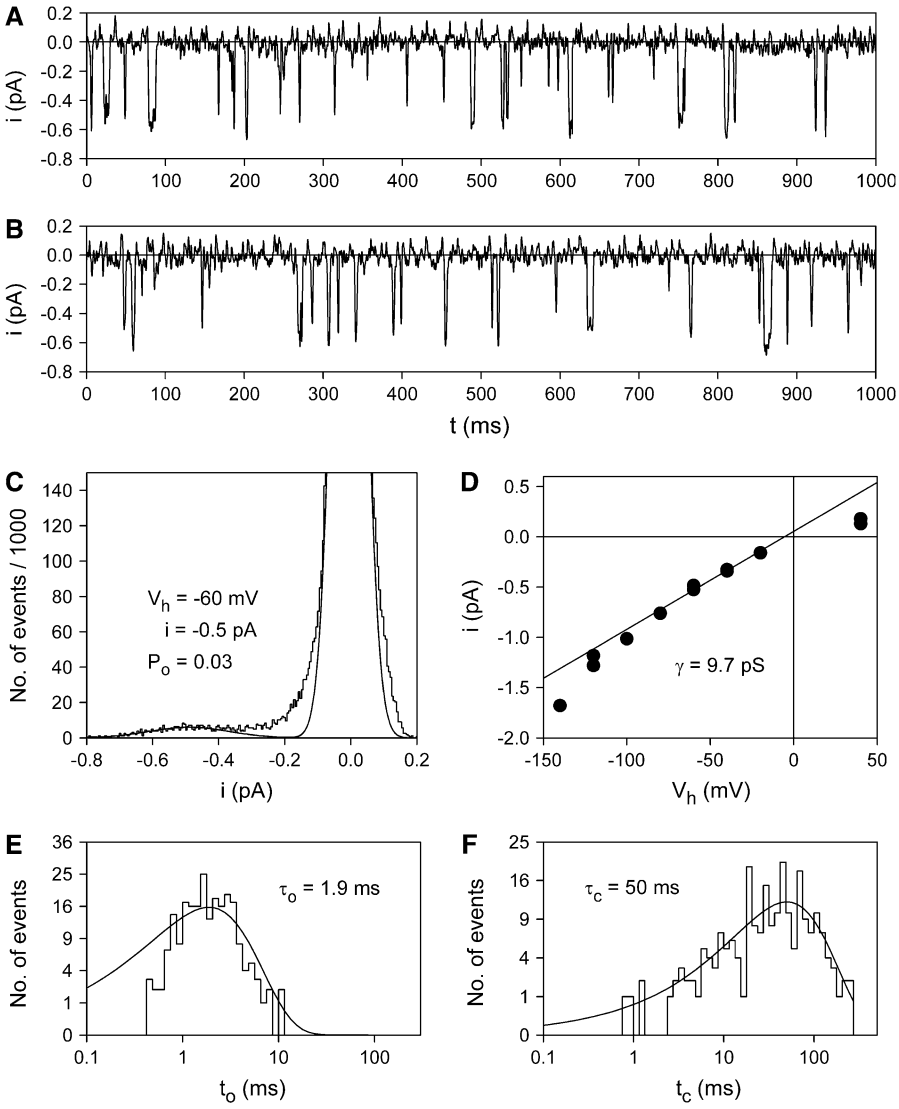

FIGURE 10 Behavior of $P2X_7$-dependent single channels in a patch of an intact oocyte. Example of a patch-clamp record in the cell-attached mode. As pipette solution, a U-tube solution containing 0.1 mM ATP^{4-} was used. (*A*, *B*) Example current traces recorded 3 and 10 min after formation of the gigaseal, respectively. $V_h = -60$ mV. (*C*, *E*, *F*) Amplitude, open and closed time histogram, respectively, of the record obtained between 10 and 10.5 min after gigaseal formation. (*D*) Current-voltage relationship of the same patch. The slope conductance was determined by a linear fit of the data between −80 and −20 mV.

the nonspecific current could be easily distinguished in the excised patch configuration from the $P2X_7$ channel currents by its comparably slow time course of onset and offset and its fully reversible nature. In the whole cell configuration, however, where the rate of solution exchange is slower than in the excised patch configuration, the nonspecific current component may bias ATP^{4-}-induced currents. At 1 mM ATP^{4-} and a leak current of 10 pA at −120 mV (corresponding to a seal resistance of ~12 GΩ if linearly related to the applied voltage), the nonspecific current amounts to ~5 pA (Fig. 2 *D*), which represents a significant background contribution to the measured current, particularly when $P2X_7$ receptor expression is low.

Single channel kinetic measurements

In contrast to most whole cell currents assigned to $P2X_7$ receptor activation (2,9,11,13–15,17–19,31), single $P2X_7$ channel currents obey rather simple and fast activation and deactivation kinetics. There are at least two possible explanations for the discrepancy between these observations. First, the $P2X_7$ receptor may be subjected to modulation by cellular constituents such as second messengers or kinases as long as the internal milieu of the cell is relatively unperturbed by the electrophysiological recordings. Particularly in the excised patch configuration, the complete washout of cellular constituents may be accompanied by a loss of a specific function. However, in contrast to this view, the $P2X_7$ receptor-mediated current kinetics were similar in the cell-attached and outside-out patch configurations. Since cell-attached patches retain intracellular constituents, washout alone cannot fully account for the observed changes in current kinetics. Second, additional ionic conductances may be induced in the whole cell configuration. An obvious candidate mechanism for the activation of such conductances is the increase in the intracellular Ca^{2+} concentration ($[Ca^{2+}]_i$).

In the excised patch-clamp experiments, Ca^{2+} in the pipette solution was buffered to low levels by EGTA and BAPTA. Moreover, unlike in whole cell current experiments, the single channel events occurring in the excised patches are probably not accompanied by a large-scale Ca^{2+} flux across the cell membrane. In fact, in whole cell voltage clamp measurements carried out with strong $[Ca^{2+}]_i$ buffering in human B lymphocytes (4) or in experiments using reduced extracellular Ca^{2+} concentration (7,11,20), simple $P2X_7$ receptor-mediated current kinetics were observed. Furthermore, a comparison between ATP-induced currents recorded in cell-attached and whole cell configurations provided evidence that Ca^{2+} is involved as a second messenger in the $P2X_7$ receptor-mediated pore formation (32). Species differences may also play a significant role, because kinetics are more complex in studies of the rat $P2X_7$ receptor (2,14, 15,17,19) than of the human $P2X_7$ receptor (4,9,11).

Based on single $P2X_7$ channel activation, an EC_{50} of ~0.3 mM ATP^{4-} was obtained, which compares well with similar values found in whole cell recordings for recombinant or native $P2X_7$ (P2Z) receptors of mice (7,20,31), toad (5), and human (4,11). In contrast, the rat $P2X_7$ receptor seems to be activated by ATP^{4-} with a higher potency, with EC_{50} values as low as 3–30 μM (2,14). From two-electrode voltage clamp recordings of human $P2X_7$ receptors expressed in *Xenopus* oocytes, we obtained evidence for distinct ATP^{4-} binding (activation) sites (12). At the single channel level, the ATP^{4-} binding site leading to $P2X_7$ channel activation seems to correspond to the low affinity site with an EC_{50} of 0.3 mM ATP^{4-}.

Long-lasting single channel openings

In whole cell current recordings, delayed deactivation was frequently observed after repetitive or sustained $P2X_7$ receptor activation by high ATP concentrations (2,9,18,19). The appearance of slowly deactivating currents was mostly accompanied by a loss of selectivity of the channel pore for small inorganic cations as indicated by a time-dependent increase in the permeability to large organic cations such as $Tris^+$ and $NMDG^+$. This phenomenon has been attributed to a progressive increase in the diameter (dilation) of the cation-conducting pore of the $P2X_7$ receptor from initially 7 Å to up to 40 Å (21). Using similar sustained activation protocols in the single channel configuration, we recorded, particularly at high ATP^{4-} concentrations, a second single channel component characterized by longer lasting channel openings than usual and a slower deactivation time course, which could reflect pore dilatation. However, no long openings were observed during sustained activation by ATP^{4-} when extracellular Na^+ was replaced by $Tris^+$, indicating that the long openings are not associated with an increase in pore diameter to a $Tris^+$-permeable size. We conclude that the apparent pore dilatation of $P2X_7$ receptors observed in macroscopic current recordings (21,23) has no equivalent at the single channel level, suggesting further that the $P2X_7$ receptor-induced permeability increase is secondary to $P2X_7$ receptor activation. Abrupt changes in open times (as observed here) or closed times or both, despite constant experimental conditions, is a characteristic of many ion channels including acetylcholine receptors (33) and NMDA receptors (34) that is designated as modal gating. From this we suggest that the transitions between short and long openings reflect a modal gating behavior of the $hP2X_7$ receptor rather than a change in the permeation characteristics to cations.

The wide scattering of open probabilities and mean shut times was found to be largely attributable to the biological variability between oocytes of different donors and, to a lesser extent, to the variability between different patches from the same oocyte. Metabolic modifications such as the phosphorylation state of the receptor may account for this variability. Tyrosine phosphorylation, in particular, has been shown to influence the amplitude and time course of $P2X_7$ receptor-dependent whole cell currents (16). The appearance of long-lasting channel openings may reflect metabolic modifications that are obviously independent of soluble intracellular components, as they occurred with outside-out patches. Accordingly, long-lasting openings were clearly related with particular batches of oocytes.

Kinetic model of $P2X_7$ receptor channel gating

The timescale of ~20 ms for activation and deactivation of the short openings of the $P2X_7$ receptor is too fast to be resolved in the whole cell configuration. However, using the outside-out configuration, we were able to measure the macroscopic and microscopic kinetics of the channel and to describe them by a C-C-C-O model (Eq. 8), which was kept as simple as possible. The mean number of shuttings per burst, which is given by the rate constants for forward and backward reactions from the C_3 state to O and C_2 states (35), respectively, was calculated to be $66/100 = 0.66$. This suggests that the $P2X_7$ receptor does not exhibit a pronounced bursting behavior, which is consistent with the experimental data. It should be mentioned, however, that other ligand-gated ion channels such as nicotinic and glycine channels show a component of very short shut times in the range of 10–30 μs (27). Since the small amplitude of $hP2X_7$ single channel events necessitated relatively strong filtering, such very short shut times would remain completely undetected. In the case that $P2X_7$ receptor channels also contain such a short shut time component, the ''open times'' would have to be interpreted as burst lengths.

Further support for a nonbursting behavior comes from the calculation of autocorrelation functions of the measured dwell times: for patches without long openings, no correlations between adjacent open or closed times were found. This also argues against the existence of additional open configurations that would be, in principle, detectable by our method. The significant correlations found for patches with

long openings may be interpreted as switching between long-lasting sojourns either in short or long opening gating modes.

The largest deviation of the experimental data from the model exists for the mean closed times at low ATP^{4-} concentrations. Seemingly, the detection of dwell times with a maximum of 500 ms due to our recording procedure is the main reason. At 10 μM ATP^{4-}, the mean shut times are estimated to be on the order of several seconds. Measurements of such long shut times would need very long-term recording in the single channel configuration, which can hardly be achieved, even though a few patches were stable for almost 1 h. Furthermore, at high activating ATP^{4-} concentrations, the activation time course was found to be slower than predicted by the model. Although the solution exchange setup used is the fastest repeatable system known, we cannot rule out entirely the possibility that the solution exchange rate was limiting for such high concentration jumps. Also, small fluctuations of the position of the liquid filament due to slightly inconstant U-tube or bathing chamber flows may lead to small deviations of the onset of ATP^{4-} application and washout. This may tend to blur, and therefore slow down, the measured activation and deactivation time courses of averaged currents, which were used for the analysis of the macroscopic channel kinetics.

We did not attempt to model the kinetics of the long-lasting openings, since they occurred too infrequently and the activation mechanisms appeared to be very complex (see Fig. 3). In principle, long-lived openings might be described by an additional open state that is entered and left with small rate constants, thus explaining slow activation, deactivation, and long mean open times.

Descriptions of the kinetics on the single receptor/channel level of heterologously expressed P2X receptors are available so far only for $P2X_2$ receptors (36) and, at least in part, for $P2X_4$ receptors (37). Except for the slight inward rectification, the fast activation by ATP, and the similar single channel conductance of the $P2X_4$ receptor, the $P2X_2$ and $P2X_4$ receptors display characteristics different from those of the $P2X_7$ receptor. In particular, the large mean open time of $\sim$5 ms seems typical for the $P2X_7$ receptor. The ATP-dependent single channel current characteristics measured in human lymphocytes (30) are indistinguishable from those shown here, corroborating the view that the native human P2Z receptor is a genuine $P2X_7$ receptor. The identical channel behavior in native cells and a recombinant system suggests further that the basic electrophysiological properties of the $P2X_7$ receptor remain unchanged upon heterologous expression in *Xenopus* oocytes.

The proposed C-C-C-O model describes the most proximal receptor activation events after ATP binding. It may help to separate genuine $P2X_7$ receptor-mediated currents from downstream effects produced by activation of intracellular or membrane-delimited pathways, as implicated by both the complex whole cell kinetics and the multiple intracellular interaction partners of the $P2X_7$ receptor (16,38,39).

SUPPLEMENTARY MATERIAL

An online supplement to this article can be found by visiting BJ Online at http://www.biophysj.org.

This work was supported by grants of the Deutsche Forschungsgemeinschaft (No. Ma1581/12-1 to F.M. and No. Schm536/6-1 to G.S.) and the Roux Program of the medical faculty of the Martin-Luther-University (Roux No. 5/09, No. 10/01, and No. 13/07 to F.M.).

REFERENCES

1. Di Virgilio, F., P. Chiozzi, D. Ferrari, S. Falzoni, J. M. Sanz, A. Morelli, M. Torboli, G. Bolognesi, and O. R. Baricordi. 2001. Nucleotide receptors: an emerging family of regulatory molecules in blood cells. *Blood.* 97:587–600.
2. Surprenant, A., F. Rassendren, E. Kawashima, R. A. North, and G. Buell. 1996. The cytolytic P_{2Z} receptor for extracellular ATP identified as a P_{2X} receptor ($P2X_7$). *Science.* 272:735–738.
3. North, R. A. 2002. Molecular physiology of P2X receptors. *Physiol. Rev.* 82:1013–1067.
4. Bretschneider, F., M. Klapperstück, M. Löhn, and F. Markwardt. 1995. Nonselective cationic currents elicited by extracellular ATP in human B-lymphocytes. *Pflugers Arch.* 429:691–698.
5. Ugur, M., R. M. Drummond, H. Zou, P. H. Sheng, J. J. Singer, and J. V. Walsh. 1997. An ATP-gated cation channel with some P2Z-like characteristics in gastric smooth muscle cells of toad. *J. Physiol. (Lond.).* 498:427–442.
6. Zou, H., M. Ugur, R. M. Drummond, and J. J. Singer. 2001. Coupling of a P2Z-like purinoceptor to a fatty acid-activated K^+ channel in toad gastric smooth muscle cells. *J. Physiol. (Lond.).* 534:59–70.
7. Colomar, A., and T. Amedee. 2001. ATP stimulation of $P2X_7$ receptors activates three different ionic conductances on cultured mouse Schwann cells. *Eur. J. Neurosci.* 14:927–936.
8. Nuttle, L. C., and G. R. Dubyak. 1994. Differential activation of cation channels and non-selective pores by macrophage P_{2z} purinergic receptors expressed in *Xenopus* oocytes. *J. Biol. Chem.* 269:13988–13996.
9. Rassendren, F., G. N. Buell, C. Virginio, G. Collo, R. A. North, and A. Surprenant. 1997. The permeabilizing ATP receptor, $P2X_7$—cloning and expression of a human cDNA. *J. Biol. Chem.* 272:5482–5486.
10. Humphreys, B. D., C. Virginio, A. Surprenant, J. Rice, and G. R. Dubyak. 1998. Isoquinolines as antagonists of the $P2X_7$ nucleotide receptor: high selectivity for the human versus rat receptor homologues. *Mol. Pharmacol.* 54:22–32.
11. Klapperstück, M., C. Büttner, T. Böhm, G. Schmalzing, and F. Markwardt. 2000. Characteristics of $P2X_7$ receptors from human B lymphocytes expressed in *Xenopus* oocytes. *Biochim. Biophys. Acta.* 1467:444–456.
12. Klapperstück, M., C. Büttner, G. Schmalzing, and F. Markwardt. 2001. Functional evidence of distinct ATP activation sites at the human $P2X_7$ receptor. *J. Physiol. (Lond.).* 534:25–35.
13. Li, Q., X. Luo, and S. Muallem. 2005. Regulation of the P2X7 receptor permeability to large molecules by extracellular Cl^- and Na^+. *J. Biol. Chem.* 280:26922–26927.
14. Petrou, S., M. Ugur, R. M. Drummond, J. J. Singer, and J. V. Walsh. 1997. $P2X_7$ purinoceptor expression in *Xenopus* oocytes is not sufficient to produce a pore-forming P2Z-like phenotype. *FEBS Lett.* 411:339–345.
15. Virginio, C., D. Church, R. A. North, and A. Surprenant. 1997. Effects of divalent cations, protons and calmidazolium at the rat $P2X_7$ receptor. *Neuropharmacology.* 36:1285–1294.
16. Kim, M., L. H. Jiang, H. L. Wilson, R. A. North, and A. Surprenant. 2001. Proteomic and functional evidence for a $P2X_7$ receptor signaling complex. *EMBO J.* 20:6347–6358.
17. Jiang, L. H., F. Rassendren, A. MacKenzie, Y. H. Zhang, A. Surprenant, and R. A. North. 2005. N-methyl-D-glucamine and

propidium dyes utilize different permeation pathways at rat $P2X_7$ receptors. *Am. J. Physiol.* 289:C1295–C1302.

18. Chessell, I. P., C. B. A. Grahames, A. D. Michel, and P. P. A. Humphrey. 2001. Dynamics of $P2X_7$ receptor pore dilation: pharmacological and functional consequences. *Drug Dev. Res.* 53:60–65.
19. Smart, M. L., B. Gu, R. G. Panchal, J. Wiley, B. Cromer, D. A. Williams, and S. Petrou. 2003. $P2X_7$ receptor cell surface expression and cytolytic pore formation are regulated by a distal C-terminal region. *J. Biol. Chem.* 278:8853–8860.
20. Chessell, I. P., A. D. Michel, and P. P. A. Humphrey. 1997. Properties of the pore-forming $P2X_7$ purinoceptor in mouse NTW8 microglial cells. *Br. J. Pharmacol.* 121:1429–1437.
21. Virginio, C., A. MacKenzie, R. A. North, and A. Surprenant. 1999. Kinetics of cell lysis, dye uptake and permeability changes in cells expressing the rat $P2X_7$ receptor. *J. Physiol.* (*Lond.*). 519:335–346.
22. Di Virgilio, F. 1995. The P2Z purinoceptor: an intriguing role in immunity, inflammation and cell death. *Immunol. Today.* 16:524–528.
23. Boldt, W., M. Klapperstück, C. Büttner, S. Sadtler, N. Schmalzing, and F. Markwardt. 2003. $Glu^{496}Ala$ polymorphism of human $P2X_7$ receptor does not affect its electrophysiological phenotype. *Am. J. Physiol.* 284:C749–C756.
24. Bretschneider, F., and F. Markwardt. 1999. Drug-dependent ion channel gating by application of concentration jumps using U-tube technique. *Methods Enzymol.* 294:180–189.
25. Markwardt, F., and G. Isenberg. 1992. Gating of maxi K^+ channels studied by Ca^{2+} concentration jumps in excised inside-out multi-channel patches (myocytes from guinea pig urinary bladder). *J. Gen. Physiol.* 99:841–862.
26. Sigworth, F. J., and S. M. Sine. 1987. Data transformations for improved display and fitting of single-channel dwell time histograms. *Biophys. J.* 52:1047–1054.
27. Colquhoun, D., and B. Sakmann. 1985. Fast events in single channel currents activated by acetylcholine and its analogues at the frog muscular endplate. *J. Physiol.* (*Lond.*). 369:501–557.
28. Schubert, R. 1996. Multiple ligand-ion solutions: a guide for solution preparation and computer program understanding. *J. Vasc. Res.* 33:86–98.
29. Colquhoun, D., and A. G. Hawkes. 1977. Relaxation and fluctuations of membrane currents that flow through drug-operated channels. *Proc. R. Soc. Lond. B Biol. Sci.* 199:231–262.
30. Markwardt, F., M. Löhn, T. Böhm, and M. Klapperstück. 1997. Purinoceptor-operated cationic channels in human B lymphocytes. *J. Physiol.* (*Lond.*). 498:143–151.
31. Nuttle, L. C., C. El-Moatassim, and G. R. Dubyak. 1993. Expression of the pore-forming P_{2z} purinoreceptor in *Xenopus* oocytes injected with $poly(A)^+$ RNA from murine macrophages. *Mol. Pharmacol.* 44:93–101.
32. Faria, R. X., F. P. DeFarias, and L. A. Alves. 2005. Are second messengers crucial for opening the pore associated with $P2X_7$ receptor? *Am. J. Physiol.* 288:C260–C271.
33. Auerbach, A., and C. J. Lingle. 1986. Heterogeneous kinetic properties of acetylcholine receptor channels in *Xenopus* myocytes. *J. Physiol.* (*Lond.*). 378:119–140.
34. Magleby, K. L. 2004. Modal gating of NMDA receptors. *Trends Neurosci.* 27:231–233.
35. Colquhoun, D., and A. G. Hawkes. 1981. On the stochastic properties of single ion channels. *Proc. R. Soc. Lond. B Biol. Sci.* 211:205–235.
36. Ding, S. H., and F. Sachs. 1999. Single channel properties of $P2X_2$ purinoceptors. *J. Gen. Physiol.* 113:695–719.
37. Negulyaev, Y. A., and F. Markwardt. 2000. Block by extracellular Mg^{2+} of single human purinergic $P2X_4$ receptor channels expressed in human embryonic kidney cells. *Neurosci. Lett.* 279:165–168.
38. Wilson, H. L., S. A. Wilson, A. Surprenant, and R. A. North. 2002. Epithelial membrane proteins induce membrane blebbing and interact with the $P2X_7$ receptor C terminus. *J. Biol. Chem.* 277:34017–34023.
39. Adinolfi, E., M. Kim, M. T. Young, F. Di Virgilio, and A. Surprenant. 2003. Tyrosine phosphorylation of HSP90 within the $P2X_7$ receptor complex negatively regulates $P2X_7$ receptors. *J. Biol. Chem.* 278: 37344–37351.